PHYSICAL REVIEW B VOLUME 15, NUMBER 5 1 MARCH 1977

Orientation dependence of motion-induced nuclear spin relaxation in single crystals

D. Wolf
Department of Physics, University of Utah, Salt Lake City, Utah 84112

D. R. Figueroa* and J. H. Strange
The Physics Laboratory, The University, Canterbury, Kent, United Kingdom
(Received 25 June 1976)

Starting from Eisenstadt and Redfield's encounter model, the dipolar pair correlation functions governing the NMR relaxation behavior in crystals may be calculated for some arbitrary (correlated or uncorrelated) self-diffusion mechanism. In several temperature and field ranges, these correlation functions allow prediction of the variation of the relaxation times T_1, T_2, and $T_{1\rho}$ as a function of the crystallographic orientation of the Zeeman field $\vec{H}_0$ and of temperature for a given self-diffusion mechanism. In the theoretical part of the present article, the encounter model is applied to a monovacancy and an interstitialcy mechanism of self-diffusion of the anions in a fluorite lattice. The theoretical predictions for the anisotropies and the actual values of T_1, T_2, and $T_{1\rho}$ in the different regions are compared with those for a random-walk mechanism of self-diffusion in a single-crystalline simple cubic lattice. In single crystals of barium fluoride, the orientation dependence of T_1, T_2, and $T_{1\rho}$ has been investigated in several temperature and field regions. To affect the dominant diffusion mechanism, the experiments included also La^{3+}- and K^+-doped samples of barium fluoride. The comparison of the anisotropy measurements with our theoretical calculations rules out random-walk diffusion as a mechanism causing the relative jumps of the fluorine ions. Although the differences in the anisotropy of T_1, T_2, and $T_{1\rho}$ predicted for vacancy and interstitialcy diffusion in fluorites were found to require too high an experimental precision for the unambiguous identification of the dominant diffusion mechanism, this theoretical and experimental investigation has confirmed all of the basic predictions of the encounter-model theory and its application to fluorites.

I. INTRODUCTION

It has been known for many years that nuclear-magnetic-resonance (NMR) relaxation experiments allow the systematic investigation of diffusion processes in crystals. The *activation energy* associated with a diffusion mechanism causing relative jumps of nuclear spins may, for example, be determined from a logarithmic plot of the spin-lattice relaxation time T_1, the spin-spin relaxation time T_2, or the spin-lattice relaxation time $T_{1\rho}$ in the rotating frame, as a function of inverse temperature.

To determine values of the underlying *diffusion coefficient D* at a given temperature, considerable theoretical efforts have to be made to relate the measured relaxation times to some assumed microscopic mechanism of motion. This procedure yields a value of the mean time τ between successive jumps of an atom, which may then be related to the corresponding diffusion coefficient at that temperature by the Einstein-Smoluchovsky relation. Owing to the uncertainties in identifying *all* (diffusion-dependent and motion-independent) contributions to the observed values of the relaxation times, diffusion coefficients thus determined are liable to error. Also, such measurements alone do not identify the diffusion mechanism.

In fact, nuclear spin relaxation studies may provide insight into the microscopic *mechanisms* causing spins to move relative to each other. This involves, however, a detailed study of the relaxation-time dependence on parameters such as the temperature or the crystallographic orientation of the large constant Zeeman field $\vec{H}_0$, thus making the experiments more tedious. Two such effects have been found to be fairly sensitive functions of the diffusion mechanism:

(i) As first outlined by Ailion and Ho,[1] in single crystals $T_{1\rho}$ depends strongly on both the orientation of the field $\vec{H}_0$ with respect to the principal crystal axes and on the diffusion mechanism. In the "strong-collision" (Slichter-Ailion[2]) region this effect has been illustrated theoretically for several self-diffusion mechanisms.[1] Previously, Eisenstadt and Redfield[3] had found that T_1 and T_2 are functions of the crystallographic orientation of $\vec{H}_0$. Their investigation of uncorrelated random-walk diffusion in a cubic crystal lattice, closely related to the theory of Torrey,[4] also showed that the anisotropies of T_1 and T_2 are dependent on temperature. A more comprehensive analysis of diffusion-induced anisotropies of T_1, T_2, and $T_{1\rho}$ in both large and small relaxation fields has been developed from the ideas of Ailion and Ho[1] and Eisenstadt and Redfield[3] using Eisenstadt and Redfield's "encounter model" for both "weak" and "strong" collisions.[2] This treatment[5,6] includes the correlation effects associated with various point-defect mechanisms of self-diffusion.

(ii) In polycrystalline or powdered samples often used to overcome the skin-effect problem in metals, anisotropies of relaxation times cannot be investigated. It was predicted recently,[5,7] however, that in both single- and polycrystalline samples shape and width of the T_1 and $T_{1\rho}$ minimum as a function of temperature are strongly influenced by correlations between successive atomic jumps. By this method correlated vacancy-induced self-diffusion may possibly be distinguished from an uncorrelated random-walk diffusion mechanism involving random atomic jumps on a crystal lattice.[8]

The object of the present work is to apply and to check experimentally some of the general predictions on anisotropies and their temperature dependences following from the comprehensive theory of these effects due to Wolf.[5-7] Similar investigations of shape and width of the T_1 and $T_{1\rho}$ minimum will be discussed elsewhere.[9]

Both calcium and barium fluoride crystals contain only one predominant type of nuclear spin, namely ^{19}F. Because of the absence of quadrupolar effects ($I=\frac{1}{2}$) and the availability of single-crystalline samples, these fluorites represent ideal systems for the study of anisotropies of T_1, T_2, and $T_{1\rho}$, both experimentally and theoretically. Also, by appropriate doping, the dominant diffusion mechanism in fluorites may be influenced in a predictable way. For that purpose, the encounter-model approach by Wolf[5,6] has been applied to the two most likely self-diffusion mechanisms in a fluorite lattice, namely, the diffusion via monovacancies and interstitialcy diffusion. After a brief review of the basic theories, the corresponding theoretical predictions for these two diffusion mechanisms will be discussed. Mainly for reasons associated with the greater purity with which BaF_2 single crystals may be grown, the experimental results presented in Sec. III, which verify our theoretical predictions, have been obtained using BaF_2 samples.

II. THEORY

A. Anisotropies of relaxation rates in cubic single crystals

Usually the Zeeman field $\vec{H}_0$ is much larger than the dipolar local field H_D in the laboratory frame, and both T_1 and T_2 are completely determined[10,11] by the spectral density functions $J^{(q)}(\omega)$ of the dipolar pair correlation functions,[5]

$$G^{(q)}(t)=\sum_{\vec{r}_m^{\,0}}\sum_{S=0}^{\infty}\frac{R_S^{(q)}(\vec{r}_m^{\,0})}{S!}\left(\frac{t}{\tau_{\mathrm{NMR}}}\right)^S\exp\left(-\frac{t}{\tau_{\mathrm{NMR}}}\right), \tag{2.1}$$

associated with a given self-diffusion mechanism. Here, τ_{NMR} denotes the mean time between consecutive "encounters," while the factors $R_S^{(q)}(\vec{r}_m^{\,0})$ specified below are closely related to the average change of the dipolar interaction of an arbitrary spin pair during S encounters. In the special case of uncorrelated random-walk diffusion on a crystal lattice, the correlation functions (2.1) were shown[5,7] to be identical to Eisenstadt and Redfield's[3] functions for systems containing only one spin type, and with the correlation functions of Torrey.[4]

In the rotating reference frame two temperature regions have to be distinguished. In the so-called weak-collision (motionally narrowed) region defined by the conditions $\tau \ll T_2^{\mathrm{RL}}$ and $H_1 \gg H_{D\rho}$, Look and Lowe[12] showed that $T_{1\rho}$ is also governed by the Fourier spectra of $G^{(q)}(t)$. In the strong-collision (Slichter-Ailion[2]) region for which $\tau \gg T_2^{\mathrm{RL}}$ and $H_1 \lesssim H_{D\rho}$, $T_{1\rho}$ was recently shown[13,14] to be related to the first time derivative of $G^{(0)}(t)$ at $t=0$. Here, T_2^{RL} denotes the spin-spin relaxation time in a "rigid" lattice, while H_1 and $H_{D\rho}$ symbolize the amplitude of the rotating and the local field, respectively.

Using the form (2.1) of $G^{(q)}(t)$, all relaxation properties of interest (e.g., temperature and orientation dependence of T_1, T_2, and $T_{1\rho}$) may be expressed in terms of the lattice factors $R_S^{(q)}(\vec{r}_m^{\,0})$ over products of the geometrical part $F_{im}^{(q)}(\vec{r}_m^{\,0})$ associated with the dipolar interaction between a pair of spins i and m,[11] before their relative movements separated by a lattice vector $\vec{r}_m^{\,0}$. These lattice factors, defined by

$$R_S^{(q)}(\vec{r}_m^{\,0})=F_{im}^{(q)}(\vec{r}_m^{\,0})\sum_{\vec{r}_m^{\,*}}W_S(\vec{r}_m^{\,0},\vec{r}_m^{\,*})F_{im}^{(q)*}(\vec{r}_m^{\,0}+\vec{r}_m^{\,*}), \tag{2.2}$$

are determined by the conditional probabilities $W_S(\vec{r}_m^{\,0},\vec{r}_m^{\,*})$ that the "relative displacement vector" of i and m due to S encounters with a point defect[5] is equal to $\vec{r}_m^{\,*}$, if the initial vector from the "representative" spin i (located at the origin of a Cartesian crystallographic coordinate system) to some spin m in its surroundings was equal to $\vec{r}_m^{\,0}$. Obviously, the probabilities $W_S(\vec{r}_m^{\,0},\vec{r}_m^{\,*})$ depend on the self-diffusion mechanism. For $S=0$ all but the rigid-lattice probabilities $W_0(\vec{r}_m^{\,0},0)$ (which are equal to unity for any vector $\vec{r}_m^{\,0}$) must vanish.[5] Consequently, the terms $R_0^{(q)}(\vec{r}_m^{\,0})$ are independent of the diffusion mechanism and characterized by the properties of a rigid lattice.

In *cubic* single crystals, the orientation dependence of $R_S^{(q)}(\vec{r}_m^{\,0})$ may be expressed in terms of the new orientation-independent lattice factors $C_S^{(q)}(\vec{r}_m^{\,0})$ and $D_S^{(q)}(\vec{r}_m^{\,0})$, which depend only on the crystallographic coordinates of spin m with respect to i

and the probabilities $W_S(\vec{r}_m^0, \vec{r}_m^*)$,[5-7] and the "anisotropy function"

$$f(\theta, \phi) = \sin^2 2\theta + \sin^4\theta \sin^2 2\phi = 2\left(1 - \sum_{p=x,y,z} \alpha_p^4\right) \tag{2.3}$$

describing the crystallographic orientation of the Zeeman field $\vec{H}_0$ in terms of the polar angle θ and the azimuthal angle ϕ.[7] The second part of Eq. (2.3) relates $f(\theta, \phi)$ to the cosine directors α_p of $\vec{H}_0$. Values of $f(\theta, \phi)$ for several principal orientations of $\vec{H}_0$ are listed in Table I.

In cubic crystals, Eq. (2.2) may therefore be rewritten as follows[5,7]:

$$R_S^{(q)}(\vec{r}_m^0) = C_S^{(q)}(\vec{r}_m^0) + f(\theta, \phi) D_S^{(q)}(\vec{r}_m^0). \tag{2.4}$$

The "magnetic" correlation time τ_{NMR} appearing in Eq. (2.1) characterizes the mean time between successive changes of the dipolar interaction between spin i and some spin m. In terms of the mean time τ between successive jumps of an atom (henceforth called the "mean jump time"), we may write[5]

$$\frac{1}{\tau_{\mathrm{NMR}}} = \frac{2}{\tau} \frac{1}{Z(0) + Z(\vec{r}_m^0)}, \tag{2.5}$$

where $Z(0)$ and $Z(\vec{r}_m^0)$ denote the average number of jumps of the "representative" spin i and spin m, respectively, that result from one encounter with the same point defect. $Z(\vec{r}_m^0)$ is known to decrease as the number of encounters, S, increases,[5] an effect attributed to the average increase of the distance $|\vec{r}_m^0|$ between the two spins. Denoting the average total number of relative jumps of i and m in S encounters by $\bar{Z}_{\mathrm{NMR}}^{(S)}(\vec{r}_m^0)$ [for $S=1$, e.g., $\bar{Z}_{\mathrm{NMR}}^{(1)}(\vec{r}_m^0) = Z(0) + Z(\vec{r}_m^0)$], Eq. (2.5) has to be rewritten as follows:

$$\frac{1}{\tau_{\mathrm{NMR}}^{(S)}} = \frac{2}{\tau} \frac{1}{\bar{Z}_{\mathrm{NMR}}^{(S)}(\vec{r}_m^0)}, \tag{2.6}$$

thus illustrating clearly that τ_{NMR} is a function of S *and* $\vec{r}_m^0$. Analogous to the practical determination of the probabilities $W_S(\vec{r}_m^0, \vec{r}_m^*)$ for $S>1$, $\bar{Z}_{\mathrm{NMR}}^{(S)}(\vec{r}_m^0)$ may be computed recursively,[5] starting from the values of $W_1(\vec{r}_m^0, \vec{r}_m^*)$, $Z(0)$, and $Z(\vec{r}_m^0)$ governed by a single encounter.

TABLE I. Numerical values of the "anisotropy function" $f(\theta, \phi)$ for different orientations of $\vec{H}_0$ and for polycrystalline or powdered samples obtained by averaging over the solid angle (Refs. 5 and 7).

$\langle hkl \rangle$	$\sum \alpha_q^4$	$f(\theta, \phi)$	θ for $\phi = \frac{1}{4}\pi$
$\langle 100 \rangle$	1	0	0°
$\langle 110 \rangle$	$\frac{1}{2}$	1	90°
$\langle 111 \rangle$	$\frac{1}{3}$	$\frac{4}{3}$	54.73°
Powder average	$\frac{3}{5}$	$\frac{4}{5}$	...

For cubic crystals at temperatures far above and far below the T_1 and $T_{1\rho}$ minimum, respectively, explicit expressions for T_1, T_2, and $T_{1\rho}$ in terms of the parameters defined above may be derived[5-7]:

Region (i): On the high-temperature side of the T_1 minimum (i.e., for $\omega_0\tau \ll 1$, $\omega_1\tau \ll 1$), Eisenstadt and Redfield[3] pointed out that all relaxation rates should be isotropic. The reason therefore lies in the quickness of the nuclear motions, i.e., the shortness of τ with respect to a Larmor precession period ω_0^{-1}. During one precession period any two spins forming a pair change their relative positions often enough to render their relative vector *after* these jumps totally independent of their relative vector *before* these jumps. As a consequence, T_1, T_2, and $T_{1\rho}$ are isotropic and equal, according to[5,7]

$$\frac{1}{T_1} = \frac{1}{T_2} = \frac{1}{T_{1\rho}} = \tfrac{3}{2}\delta\tau \sum_{S=0}^{\infty} A_1(S). \tag{2.7}$$

Here $\delta = \gamma^4\hbar^2 I(I+1)$ and the lattice sums $A_1(S)$ were defined as follows [cf. Eqs. (2.2) and (2.4)]:

$$A_1(S) = \sum_{\vec{r}_m^0} [C_S^{(1)}(\vec{r}_m^0) + C_S^{(2)}(\vec{r}_m^0)]\, \bar{Z}^{(S)}(\vec{r}_m^0). \tag{2.8}$$

It is worth noting that the values of the relaxation rates in this region consist of contributions from many encounters. Although T_1, T_2, and $T_{1\rho}$ are isotropic for this reason, due to the very same cause, their values at a given temperature are very sensitive functions of the microscopic mechanism causing diffusion.

Region (ii): For temperatures between the T_1 and the $T_{1\rho}$ minimum (i.e., for $\omega_0\tau \gg 1$, $\omega_1\tau \ll 1$), T_2 and $T_{1\rho}$ for $H_1 \gg H_{D\rho}$ are expected to be equal and strongly anisotropic, according to[5,7]

$$\frac{1}{T_2} = \frac{1}{T_{1\rho}} = \frac{3\delta\tau}{8}\left(\sum_{S=0}^{\infty} A_2(S) + f(\theta, \phi) \sum_{S=0}^{\infty} B_2(S)\right), \tag{2.9}$$

with the lattice sums

$$A_2(S) = \sum_{\vec{r}_m^0} C_S^{(0)}(\vec{r}_m^0)\, \bar{Z}_{\mathrm{NMR}}^{(S)}(\vec{r}_m^0), \tag{2.10}$$

$$B_2(S) = \sum_{\vec{r}_m^0} D_S^{(0)}(\vec{r}_m^0)\, \bar{Z}_{\mathrm{NMR}}^{(S)}(\vec{r}_m^0). \tag{2.11}$$

Obviously T_2 and $T_{1\rho}$ are still affected by *many* encounters [see Eq. (2.9)]. This is quite in con-

trast to T_1 which, in this region, is governed exclusively by terms for $S=0$ and $S=1$:

$$1/T_1 = (3\delta/2\omega_0^2\tau)[A_3 + f(\theta,\phi)B_3], \tag{2.12}$$

where the orientation-independent lattice sums A_3 and B_3 are given by

$$A_3 = \sum_{\vec{r}_m^0} \{[4C_0^{(1)}(\vec{r}_m^0) - 4C_1^{(1)}(\vec{r}_m^0) + C_0^{(2)}(\vec{r}_m^0) - C_1^{(2)}(\vec{r}_m^0)]/\overline{Z}^{(1)}(\vec{r}_m^0)\}, \tag{2.13}$$

$$B_3 = \sum_{\vec{r}_m^0} \{[3D_0^{(1)}(\vec{r}_m^0) - 3D_1^{(1)}(\vec{r}_m^0)]/\overline{Z}^{(1)}(\vec{r}_m^0)\}. \tag{2.14}$$

In writing the expression for B_3 the following relationship[5,7] was used:

$$\sum_{\vec{r}_m^0} D_S^{(2)}(\vec{r}_m^0) = -\sum_{\vec{r}_m^0} D_S^{(1)}(\vec{r}_m^0) = \frac{1}{9}\sum_{\vec{r}_m^0} D_S^{(0)}(\vec{r}_m^0). \tag{2.15}$$

The characteristic behavior of T_1 is readily understood if we note that, for $\omega_0\tau \gg 1$, during one Larmor precession period none or at the most one encounter is likely to take place. Therefore, T_1 is anisotropic, and for the same reason, it is not a very sensitive function of the diffusion mechanism.

In contrast, for the following reasons the spin-spin relaxation time in this region is anisotropic and a rather sensitive function of the mechanism causing the relative jumps of the nuclear spins: The lifetime-broadening contribution to T_2 disappears upon lowering the temperature through the T_1 minimum. This is seen from the fact that, for $\omega_0\tau \gg 1$, the spectral densities $J^{(1)}(\omega_0)$ and $J^{(2)}(2\omega_0)$ no longer contribute to T_2^{-1} [see Eqs. (2.9)–(2.11)]. Instead, T_2^{-1} is governed by the spectral densities at vanishing Larmor frequency ($\omega_0 = 0$) associated with the fluctuations of the secular dipolar interactions. This illustrates the well-known phenomenon that, in a T_2 experiment, the nuclear motions are analyzed primarily in terms of the nuclear precession in the dipolar local field and *not* in the Zeeman field $\vec{H}_0$. Consequently, in contrast to T_1^{-1}, spin-spin relaxation in this region is affected by *many* encounters [see Eqs. (2.9)–(2.11)]. Hence, T_2^{-1} is a rather sensitive function of the diffusion mechanism and is anisotropic. The same is true, of course, for $T_{1\rho}^{-1}$, since in the related experiments nuclear motions are analyzed in terms of the Larmor precession frequency ω_1 due to the rotating field H_1, which is typically orders of magnitude smaller than ω_0 but of the same order of magnitude as the local-field precession frequency.

Region (iii): For temperatures below the $T_{1\rho}$ minimum in large fields (i.e., for $\omega_1\tau \gg 1$ and $H_1 \gg H_{D\rho}$), the largest anisotropy of $T_{1\rho}$ occurs with

$$1/T_{1\rho} = (3\delta/8\omega_1^2\tau)[A_4 + f(\theta,\phi)B_4]. \tag{2.16}$$

Here, A_4 and B_4 are defined as follows:

$$A_4 = \sum_{\vec{r}_m^0} \{[C_0^{(0)}(\vec{r}_m^0) - C_1^{(0)}(\vec{r}_m^0)]/\overline{Z}_{\rm NMR}^{(1)}(\vec{r}_m^0)\}, \tag{2.17}$$

$$B_4 = \sum_{\vec{r}_m^0} \{[D_0^{(0)}(\vec{r}_m^0) - D_1^{(0)}(\vec{r}_m^0)]/\overline{Z}_{\rm NMR}^{(1)}(\vec{r}_m^0)\}. \tag{2.18}$$

Analogous to Eq. (2.12), on the low-temperature side of the $T_{1\rho}$ minimum only the terms for $S=0$ and $S=1$ contribute to $T_{1\rho}$, in contrast to the high-temperature side of this minimum [see Eq. (2.9)]. This illustrates that in a $T_{1\rho}$ experiment the relative motions of spins are analyzed in terms of the Larmor precession frequency ω_1.

Region (iv): In the Slichter-Ailion region (i.e., for $\tau \gg T_2^{\rm RL}$, $H_1 \lesssim H_{D\rho}$), assuming that between successive defect jumps a common spin temperature of the Zeeman and the dipolar reservoir may *not* be established ($\tau_d \ll T_2^{\rm RL} \ll \tau$, where τ_d denotes the mean time between defect jumps), the encounter model[6] yields the following expression for $T_{1\rho}$:

$$\frac{1}{T_{1\rho}} = \frac{H_{D\rho}^2}{H_1^2 + H_{D\rho}^2} \frac{[A_4 + f(\theta,\phi)B_4]}{[A_0^{(0)} + f(\theta,\phi)B_0^{(0)}]} \frac{2}{\tau}. \tag{2.19}$$

The lattice sums $A_0^{(0)}$ and $B_0^{(0)}$ also determine directly the anisotropy of the local field given by

$$H_{D\rho}^2 = \tfrac{1}{4}\gamma^2\hbar^2 I(I+1)\sum_{\vec{r}_m^0} R_0^{(0)}(\vec{r}_m^0) = \tfrac{1}{4}\gamma^2\hbar^2 I(I+1)[A_0^{(0)} + f(\theta,\phi)B_0^{(0)}], \tag{2.20}$$

with

$$A_0^{(q)} = \sum_{\vec{r}_m^0} C_0^{(q)}(\vec{r}_m^0), \quad B_0^{(q)} = \sum_{\vec{r}_m^0} D_0^{(q)}(\vec{r}_m^0). \tag{2.21}$$

Using the first time derivative of the correlation function (2.1) at $t=0$, Eq. (2.19) may be derived independently in terms of Wolf and Jung's low-field perturbation formalism.[13] Inserting Eq. (2.20), Eq. (2.19) may be rewritten as follows:

$$\frac{1}{T_{1\rho}} = \frac{\gamma^2\hbar^2 I(I+1)}{2\tau} \times \frac{A_4 + f(\theta,\phi)B_4}{H_1^2 + \frac{1}{4}\gamma^2\hbar^2 I(I+1)[A_0^{(0)} + f(\theta,\phi)B_0^{(0)}]}. \tag{2.22}$$

Noting that owing to the rapid decrease of the dipolar interaction between any two spins with increasing number of encounters, the rigid-lattice terms ($S=0$) in Eqs. (2.1), (2.2), and (2.4) dominate over all terms for which $S>0$, it is obvious that the largest contributions to A_4 and B_4 [see Eqs. (2.17) and (2.18)] arise from the rigid-lattice terms. Therefore, in a large H_1 field the anisotropy of $T_{1\rho}$ [see Eq. (2.16)] is mainly due to the orientation dependence (2.20) of the secular local field. In contrast, in a vanishingly small H_1 field ($H_1 \ll H_{D\rho}$), by inserting Eqs. (2.17) and (2.18) into Eq. (2.22), it is seen that without the terms for $S=1$, $T_{1\rho}$ in zero field would be completely isotropic. As a result, in the Slichter-Ailon region $T_{1\rho}$ is only moderately anisotropic but rather closely related to the particular self-diffusion mechanism. As H_1 is increased in Eq. (2.22), the orientation dependence of $T_{1\rho}$ increases sharply towards the anistropy of $H_{D\rho}^2$. However, since the $T_{1\rho}$ anisotropy is then mainly due to the motion-independent local field, it is no longer such a sensitive function of the diffusion mechanism.

In the laboratory frame, the local field is isotropic so that no similar effect occurs. This may be understood from the following: Starting from the definition of the dipolar local field by the trace relation,

$$H_D^2 = \mathrm{Tr}(\mathcal{H}_D^{\mathrm{RL}})^2/\gamma^2\hbar^2 \mathrm{Tr} I_z^2 , \tag{2.23}$$

the evaluation of the traces over the spin-operator terms in the rigid-lattice dipolar Hamiltonian $\mathcal{H}_D^{\mathrm{RL}}$ yields

$$H_D^2 = \tfrac{3}{2}\gamma^2\hbar^2 I(I+1) \sum_{\vec{r}_m^0} \left[\tfrac{1}{6}\left|F_{im}^{(0)}(\vec{r}_m^0)\right|^2 + 2\left|F_{im}^{(1)}(\vec{r}_m^0)\right|^2 + \tfrac{1}{2}\left|F_{im}^{(2)}(\vec{r}_m^0)\right|^2\right]. \tag{2.24}$$

Inserting the lattice terms (2.2) and (2.4) for $S=0$ (rigid-lattice terms), applying the relation (2.15), and using the definitions (2.21), we obtain

$$H_D^2 = \tfrac{3}{2}\gamma^2\hbar^2 I(I+1)(\tfrac{1}{6}A_0^{(0)} + 2A_0^{(1)} + \tfrac{1}{2}A_0^{(2)}) \tag{2.25}$$

for all values of θ and ϕ; i.e., H_D^2 is completely isotropic.

The application of the above expressions for T_1, T_2, and $T_{1\rho}$ to polycrystalline or powdered samples is not quite trivial in that, generally, the solid-angle averaging procedure of the decaying magnetization leads to nonexponential decay functions. However, if the exponentiality of the relaxation process is postulated, in the high-field relations (2.9), (2.12), and (2.16), $f(\theta, \phi)$ may simply be replaced by its averaged value listed in Table I.[5,7] In the Slichter-Ailion region [see Eqs. (2.19) and (2.22)] the local-field anisotropy must be included in the averaging process, thus greatly complicating the application of Eq. (2.19) to powdered materials. (This problem is discussed in detail in Ref. 6.)

B. Numerical results for self-diffusion in fluorite lattices

To obtain numerical values of the orientation dependences of T_1, T_2, and $T_{1\rho}$ for a monovacancy and an interstitialcy diffusion mechanism in a fluorite lattice, the lattice sums defined above must be evaluated. The rigid-lattice terms $A_0^{(q)}$ and $B_0^{(q)}$ governing the local fields $H_{D\rho}$ and H_D [see Eqs. (2.20), (2.21), and (2.25)] thus obtained are listed in Table II. These and all other lattice sums presented below were extended over the $11^3 = 1331$ spins closest to the representative spin i at the origin of a Cartesian crystallographic coordinate system with its principal axes parallel to the $\langle 100\rangle$ directions of the simple cubic lattice occupied by the fluorine spins. The values in Table II may be checked conveniently by evaluating the ratio[4,11]

$$\left\langle \sum_{\vec{r}_m^0} \left|F_{im}^{(0)}(\vec{r}_m^0)\right|^2 \right\rangle_{\theta,\phi} : \left\langle \sum_{\vec{r}_m^0} \left|F_{im}^{(1)}(\vec{r}_m^0)\right|^2 \right\rangle_{\theta,\phi} : \left\langle \sum_{\vec{r}_m^0} \left|F_{im}^{(2)}(\vec{r}_m^0)\right|^2 \right\rangle_{\theta,\phi}$$
$$= (A_0^{(0)} + 0.8B_0^{(0)}) : (A_0^{(1)} + 0.8B_0^{(1)}) : (A_0^{(2)} + 0.8B_0^{(2)}) = 6:1:4 . \tag{2.26}$$

The brackets $\langle\ \rangle_{\theta,\phi}$ represent an average over the solid angle, and for polycrystalline or powdered materials[7] $f(\theta, \phi) = 0.8$. Also, according to Eqs. (2.15) and (2.21), for $S=0$ the conditions

$$B_0^{(2)} = -B_0^{(1)} = \tfrac{1}{9}B_0^{(0)} \tag{2.27}$$

must be satisfied. As readily verified, the values in Table II are in accord with both Eq. (2.26) and Eq. (2.27).

The evaluation of all other lattice sums defined in Sec. II A requires the determination of the probabilities $W_1(\vec{r}_m^0, \vec{r}_m^*)$ and the mean numbers

TABLE II. Rigid-lattice sums $A_0^{(q)}$ and $B_0^{(q)}$ defined via Eqs. (2.21) and (2.4) and Ref. 7 for a simple cubic lattice occupied by the anions in a fluorite lattice. (In units of a_0^{-6}, where $2a_0$ denotes the cube edge of an elementary cell, i.e., the $F^- - F^-$ distance.)

q	$A_0^{(q)}$	$B_0^{(q)}$
0	0.2085[a]	−0.1296[a]
1	0.0060	0.0144
2	0.0814	−0.0144

[a] These values have been calculated earlier by Ailion and Ho (Ref. 1).

of jumps, $Z(0)$ and $Z(\vec{r}_m^{\,0})$, for an average encounter with a vacancy or an interstitial atom, respectively. As illustrated earlier for fcc and bcc lattices, the correlated relative motions of atoms during an encounter with randomly migrating vacancy may be simulated on a computer.[5,6] This "Monte Carlo method" involves the simulation of typically about 1000–2000 encounters, in each of which a vacancy performs about 700 random jumps on its way *to* the representative atoms (which is the only atom in this encounter to jump at least once), and the same number *after* this first jump of the representative atom.[5,6] For further details, the reader is referred to the original computer program and its description.[15]

This computer method may also be adopted to simulate encounters with interstitial atoms. The main difference to the simulation of a vacancy mechanism lies in the fact that (i) in each interstitialcy jump *two* atoms are involved, and (ii) after each interstitialcy jump the interstitial atom changes its identity, in that a different atom now occupies an interstitial site. Collinear jumps of the two moving atoms may not take place in a fluorite lattice, since the corresponding paths are blocked by the cations. In this way the parameters $W_1(\vec{r}_m^{\,0}, \vec{r}_m^{\,*})$, $Z(0)$, and $Z(\vec{r}_m^{\,0})$ have been determined, some typical values of which are shown in Table III. All simulations and lattice sums were performed on the CDC 6600 computer at the University of Stuttgart, West Germany. The simulation of 1100 encounters explained in detail in Ref. 15 requires about 10 min of computer time.

TABLE III. Some typical results of the computer simulation of an interstitialcy (Int.) and a monovacancy (Vac.) mechanism of self-diffusion in a fluorite lattice. All quantities are defined in the text.

	Vac.	Int.
$Z(0)$	1.51	1.30
$Z(\vec{r}_m^{\,0})$ for any of the G nearest neighbors	0.81	0.41
$Z(\vec{r}_m^{\,0})$ for any of the second-nearest neighbors	0.61	0.33
$W_1(\vec{r}_m^{\,0}, 0)$ (%)	18.5	9.3
$W_1(\vec{r}_m^{\,0}, \vec{r}_m^{\,*})$ for $\vec{r}_m^{\,*}$ equal to any of the G nearest-neighbor vectors (%)	12.2	5.6
$W_1(\vec{r}_m^{\,0}, \vec{r}_m^{\,*})$ for $\vec{r}_m^{\,*}$ equal to any second-nearest-neighbor vector (%)	0.6	3.2
f(simulation)	0.649	0.985
f(exact)	0.653	0.986

As illustrated by Wolf, Differt, and Mehrer,[16] the basic simulation technique also allows one to determine the geometrical correlation factor[17] f as the special case in which all pair correlations are neglected, thus investigating only the correlated jumps of the representative spin i. To check the results of our computer simulations, the values of f were determined for both diffusion mechanisms and compared to their exact values known from analytical methods.[17,18] These results have been included in Table III. The small differences between the exact values of f and our results have to be attributed to the limited number of encounters and of vacancy jumps in one encounter simulated.

The values of $Z(0)$ and $W_1(\vec{r}_m^{\,0}, 0)$ listed in Table III clearly illustrate that in an encounter with a vacancy, the "representative" atom [initially located at the origin, $\vec{r}_m^{\,0} = (0, 0, 0)$] performs a greater number of correlated jumps and is more likely to return to its original position than in an encounter of the interstitialcy type. This effect is also apparent from the much smaller value of f for the vacancy mechanism.

Using the results of these computer simulations, the geometrical probabilities and mean numbers of jumps associated with an arbitrary number S of encounters may be calculated recursively.[5,8] Thus, finally, the lattice sums governing the orientation dependence of T_1, T_2, and $T_{1\rho}$ in the temperature regions discussed above may be evaluated (see Table IV). To obtain sufficient accuracy for the summations over the total number S of encounters in Eqs. (2.7) and (2.9), it was found necessary to include the relaxation contributions from as many as $S = 10$ encounters. A further increase of S left the results listed in lines 1 and 2 of Table IV practically unchanged.

Assuming that a common spin temperature is established not only between consecutive encounters but also during consecutive defect jumps ($\tau \gg \tau_d \gg T_2^{\mathrm{RL}}$), Ailion and Ho[1] calculated the orientation dependence of $T_{1\rho}$ in zero field for a monovacancy mechanism. Their result is listed in line 7 of Table IV. To extend these considerations to the more realistic temperature region in which a common spin temperature may still be established between successive encounters but no longer between consecutive defect jumps ($\tau_d \ll T_2^{\mathrm{RL}} \ll \tau$, i.e., the temperature region where the encounter model is valid), Slichter and Ailion proposed multiplication of the low-temperature relaxation rate ($\tau_d \gg T_2^{\mathrm{RL}}$) by a factor of $(G-1)(G-2)/G^2$, where G represents the coordination number of the crys-

TABLE IV. Values of relaxation rates and anisotropy factors in the four temperature regions discussed above for a monovacancy (Vac.) and an interstitialcy (Int.) mechanism of self-diffusion for the anions in a fluorite lattice and for random-walk diffusion according to Sholl (Ref. 22). Also included are the results of Ailion and Ho (Ref. 1) for $\tau_d \gg T_2^{RL}$, and the predictions of Ho and Ailion (Ref. 19). [$\delta = \gamma^4 \hbar^2 I(I+1)$; $2a_0$ is the cube edge of a unit cell].

	Vacancy	Δ (%)	Interstitialcy	Δ (%)	Random walk (Ref. 22)	Δ (%)
$1/T_1 = 1/T_2 = 1/T_{1\rho}$ for $\omega_0\tau \ll 1$ [See Eq. (2.7)]	$0.446\delta\tau a_0^{-6}$	0	$0.284\delta\tau a_0^{-6}$	0	$0.280\delta\tau a_0^{-6}$	0
$1/T_1$ for $\omega_0\tau \gg 1$ [See Eq. (2.12)]	$[0.0521 + 0.0241 f(\theta,\phi)]\frac{\delta a_0^{-6}}{\omega_0^2\tau}$	−38	$[0.0786 + 0.0354 f(\theta,\phi)]\frac{\delta a_0^{-6}}{\omega_0^2\tau}$	−37	$[0.117 + 0.056 f(\theta,\phi)]\frac{\delta a_0^{-6}}{\omega_0^2\tau}$	−39
$1/T_2$ (for $\omega_0\tau \gg 1$) $= 1/T_{1\rho}$ (for $\omega_1\tau \ll 1$) [See Eq. (2.9)]	$[0.245 - 0.138 f(\theta,\phi)]\delta\tau a_0^{-6}$	302	$[0.158 - 0.091 f(\theta,\phi)]\delta\tau a_0^{-6}$	330	$[0.136 - 0.065 f(\theta,\phi)]\delta\tau a_0^{-6}$	176
$1/T_{1\rho}$ for $\omega_1\tau \gg 1, H_1 \gg H_{D\rho}$ [See Eq. (2.16)]	$[0.0278 - 0.0180 f(\theta,\phi)]\frac{\delta a_0^{-6}}{\omega_1^2\tau}$	631	$[0.0414 - 0.0266 f(\theta,\phi)]\frac{\delta a_0^{-6}}{\omega_1^2\tau}$	597	$[0.0637 - 0.0416 f(\theta,\phi)]\frac{\delta a_0^{-6}}{\omega_1^2\tau}$	674
$1/T_{1\rho}$ for $H_1 = 0$ and $\tau_d \ll T_2^{RL} \ll \tau$ [See Eq. (2.22)]	$\frac{2}{\tau}\frac{[0.0741 - 0.0481 f(\theta,\phi)]}{[0.2085 - 0.1296 f(\theta,\phi)]}$	27	$\frac{2}{\tau}\frac{[0.1104 - 0.0710 f(\theta,\phi)]}{[0.2085 - 0.1296 f(\theta,\phi)]}$	20	$\frac{2}{\tau}\frac{[0.1699 - 0.1109 f(\theta,\phi)]}{[0.2085 - 0.1296 f(\theta,\phi)]}$ [b]	32
$1/T_{1\rho}$ for $H_1 = 0$, and $\tau_d \ll T_2^{RL} \ll \tau$ by Ho and Ailion (Ref. 19) (Int.) and Ailion and Ho (Ref. 1) (Vac.)	$\frac{2}{\tau}\frac{[0.0774 - 0.0492 f(\theta,\phi)]}{[0.2087 - 0.1296 f(\theta,\phi)]}$ [a]	13	$\frac{2}{\tau}\frac{[0.1850 - 0.1208 f(\theta,\phi)]}{[0.2087 - 0.1296 f(\theta,\phi)]}$ [a]	33	...	
$1/T_{1\rho}$ for $H_1 = 0$, and $\tau_d \gg T_2^{RL}$ by Ailion and Ho (Ref. 1)	$\frac{2}{\tau}\frac{[0.1393 - 0.0886 f(\theta,\phi)]}{[0.2087 - 0.1296 f(\theta,\phi)]}$ [a]	13	...		...	
H_D^2 [See Eq. (2.25)]			$0.1303\delta\gamma^{-2}a_0^{-6}$			0
$H_{D\rho}^2$ [See Eq. (2.20)]			$[0.0512 - 0.0324 f(\theta,\phi)]\delta\gamma^{-2}a_0^{-6}$			540

[a] Originally these values were presented for the special case $\phi = 0$ and in units of $16a_0^{-6}\gamma^2\hbar^2$ rather than a_0^{-6}.

[b] The individual lattice sums in the denominator were taken from Table II; those in the numerator were calculated from Sholl's data (Ref. 22) in line 4 [see also Eqs. (2.19) and (2.16)].

tal. These factors, taking into account correlation effects and the "trail of hot spins" left behind by a vacancy,[1] have been incorporated in the encounter model in a more quantitative way, thus eventually leading to different orientation dependences of $T_{1\rho}$ in the two regions.[6]

Starting from the results of line 7, the anisotropy of $T_{1\rho}$ for the vacancy case in the region in which $\tau_d \ll T_2^{RL} \ll \tau$ (see column 1 of line 6) have been calculated in this approximate fashion. The results for interstitialcy diffusion in the region where $\tau_d \ll T_2^{RL} \ll \tau$ included in line 6 of Table IV were presented by Ho and Ailion,[19] using a very simplified version of the encounter model for interstitialcy diffusion in this temperature region.[20] Also included in Table IV are recent results of Sholl[22] for a random-walk mechanism of self-diffusion in a crystal lattice.

To illustrate the anisotropies of $T_{1\rho}$ in the Slichter-Ailion region predicted by the different models (see lines 5 to 7 of Table IV), in Fig. 1 $T_{1\rho}$ is plotted as a function of the polar angle θ for $\phi = 45$ deg.

The largest value of the "anisotropy function" $f(\theta, \phi)$ is $\frac{4}{3}$ (see Table I) which corresponds to the orientation of $\vec{H}_0$ along a $\langle 111 \rangle$ direction. The "anisotropy factor" Δ, defined by

$$\Delta = \frac{T_r(f(\theta,\phi)=\frac{4}{3}) - T_r(f(\theta,\phi)=0)}{T_r(f(\theta,\phi)=0)} = \frac{T_r(\langle 111\rangle) - T_r(\langle 100\rangle)}{T_r(\langle 100\rangle)}, \qquad (2.28)$$

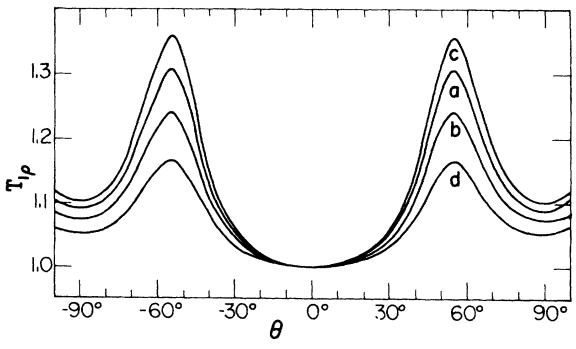

FIG. 1. Normalized orientation dependence of $T_{1\rho}$ in zero field ($H_1 = 0$) in the Slichter-Ailion region as a function of the polar angle θ for $\phi = 45°$ ($\theta = 0$ for $\vec{H}_0$ along $\langle 100 \rangle$), for (a) monovacancy diffusion ($\tau_d \ll T_2^{RL} \ll \tau$) in terms of the encounter model adopted in this article (see line 5 of Table IV); (b) interstitialcy diffusion ($\tau_d \ll T_2^{RL} \ll \tau$) in terms of the encounter model (see line 5 of Table IV); (c) interstitialcy diffusion ($\tau_d \ll T_2^{RL} \ll \tau$) [see Ho and Ailion (Ref. 19) and line 6 of Table IV]; (d) monovacancy diffusion for $\tau_d \ll T_2^{RL} \ll \tau$ in Slichter and Ailion's (Ref. 2) approximation involving the factor $(G-1)(G-2)/G^2$ (see line 6, column 1 of Table IV).

therefore, represents a convenient measure for the orientation dependence of T_1, T_2, and $T_{1\rho}$, respectively. Values of Δ for the different diffusion mechanisms have been included in Table IV. Note that Δ is referred to the relaxation *time* and not the rate. Similarly, in the bottom line of Table IV, Δ refers to the anisotropy of the inverse local field $H_{D\rho}^{-2}$.

Comparing the values of Δ in line 4 and in the bottom line of Table IV, it is observed that for $\omega_1 \tau \gg 1$, $H_1 \gg H_{D\rho}$ the anisotropy of $T_{1\rho}^{-1}$ is indeed very similar to that of the local field $H_{D\rho}^2$, since $T_{1\rho}$ and $H_{D\rho}^{-2}$ show very similar values of Δ. The reason for listing the anisotropy of $H_{D\rho}^{-2}$ actually is to illustrate this phenomenon.

III. EXPERIMENTAL RESULTS

The single crystals of barium fluoride, both pure and doped with La^{3+} ions, were grown from the melt by the Stack-Borger method using graphite crucibles heated in an rf induction furnace. The samples used were in the form of cylinders typically 2 cm in length and 1 cm in diameter. The crystallographic orientation of the cylindrical axis was determined in each case from Laue back-reflection x-ray photographs. Samples were sealed under high vacuum in quartz tubes which fitted inside an rf coil made from gold wire. The coil and sample assembly were positioned in the magnet with their axes perpendicular to the magnetic field $\vec{H}_0$ and attached to a stainless-steel head with a calibrated circular scale. The complete rf head and sample could be rotated about their axes within the water-cooled furnace jacket surrounding the sample. The orientation θ of the crystal with respect to $\vec{H}_0$ in the plane perpendicular to its cylindrical axis was measured using the circular scale to an accuracy of ±2°. Uncertainty in the determination of the true orientation of the sample's cylindrical axis introduced a possible error of ±5° in the angle ϕ.

The ^{19}F nuclear spin relaxation times were measured using a Polaron pulsed NMR spectrometer, operating at 10 MHz. T_1 was measured using a 90°-τ-90° pulse sequence. T_2 was measured from the free induction decay at low temperatures and from the spin-echo-amplitude decay using a Carr-Purcell[23] Meiboom-Gill[24] pulse sequence at higher temperatures. For the measurement of $T_{1\rho}$ the nuclear magnetization was spin-locked by applying a 90-deg pulse followed by a long pulse shifted in rf phase by 90 deg from the first pulse. In order to distinguish clearly between $T_{1\rho}$ in the high-field ($H_1 \gg H_{D\rho}$) weak-collision region and $T_{1\rho}$ in the Slichter-Ailion region ($H_1 \to 0$), $T_{1\rho}$ was always measured in rf fields H_1 of 10–12 G so that

the condition $H_1 \gg H_{D\rho}$ was always maintained. Thus measurements of $T_{1\rho}$ correspond to the weak-collision region. Measurements of $T_{1\rho}$ in the Slichter-Ailion region were made in zero H_1 field and are referred to hereafter as T_{1D}. The pulse sequence used to measure T_{1D} was that due to Jeener *et al.*[25] First, order was transferred from the Zeeman to the dipolar system by application of a 90°_x-τ-45°_y pulse pair. This was followed by an observation pulse, 45°_x, at a suitable time later. Relaxation times were measured to an accuracy of ±5% to ±10%, the T_{1D} measurements having the lower accuracy due to the inherently lower signal-to-noise ratio in the method of measurement.

Sample temperatures could be adjusted from 300 to 1300 K by means of the furnace, described elsewhere,[26,27] and temperatures were maintained constant to ±1 K throughout a set of angular-dependence measurements.

The crystal-orientation dependence of the ^{19}F relaxation times in BaF_2 has been measured over a 180° span of the angle θ. In order to investigate the systems in which vacancy and interstitialcy mechanisms of diffusion are separately dominant, some samples were doped with aliovalent cation impurities K^+ and La^{3+}. The mechanism dependence of the relaxation behavior will be discussed later, but first the general predictions of the theory will be considered.

A plot of the ^{19}F relaxation times in pure BaF_2 against reciprocal temperature is shown in Fig. 2. These measurements span the temperature range 300–1300 K and clearly show the different regions of interest, as defined in Sec. II. The measurements shown of T_1, T_{1D}, and T_2 each correspond to one sample orientation only, but $T_{1\rho}$ results for three orientations are plotted. The T_1 minimum occurs at 926 K, and well above this temperature is region (i). The observed minimum in $T_{1\rho}$ occurs at one temperature for all orientations since the frequency spectrum of the self-diffusion is independent of orientation. The variation in depth of the minimum illustrates the large anisotropy of the dipolar interaction. For the rf-field strength used, $H_1 = 12$ G, the minimum occurs at 736 K, and region (ii) corresponds to the range 736–926 K for pure BaF_2. Region (iii) is below 736 K. Region (iv), where $H_1 = 0$, is shown by the plot of T_{1D} which extends up to 626 K. In the low-temperature regions of the T_{1D} and T_1 plots, both relaxation times show a very weak temperature dependence due to relaxation associated with residual paramagnetic impurity. For the purpose of this study, these regions were avoided.

The orientation dependences of T_1, T_2, and $T_{1\rho}$ were measured at fixed temperatures where the extreme conditions $\omega_0\tau$ or $\omega_1\tau \gg 1$, and

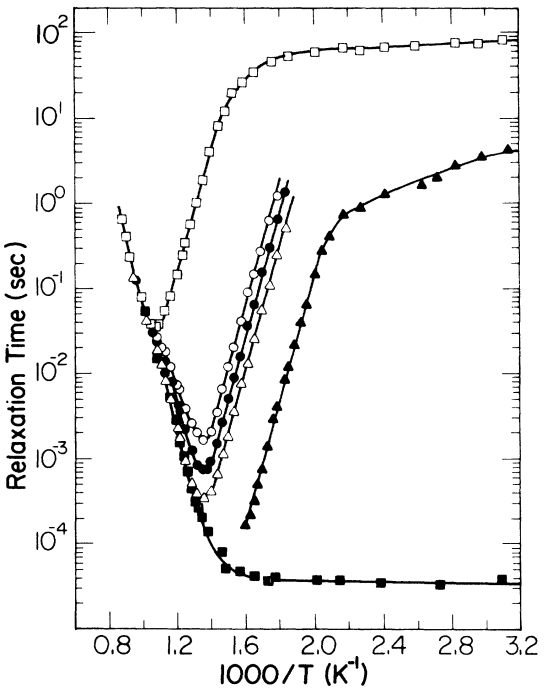

FIG. 2. Temperature dependence of ^{19}F relaxation times in pure BaF_2. □: T_1 for $\vec{H}_0 \| \langle 110 \rangle$; $T_{1\rho}$ at $H_1 = 12$ G for ○ $\vec{H}_0 \| \langle 111 \rangle$, and ● $\vec{H}_0 \| \langle 110 \rangle$, and △ $\vec{H}_0 \| \langle 100 \rangle$; ▲: T_{1D} for $\vec{H}_0 \| \langle 110 \rangle$; ■: T_2 for $\vec{H}_0 \| \langle 100 \rangle$. The lines drawn through the points have no theoretical significance.

$\omega_0\tau \ll 1$, respectively, could be fulfilled so that the numerical expressions listed in Table IV could be applied with confidence. Two distinct temperature domains are primarily distinguished which are determined by the magnitude of the ionic jump frequency τ^{-1} relative to the Larmor frequency ω_0. At elevated temperatures, the ionic jump frequency is high, and above the T_1 minimum the condition $\omega_0\tau \ll 1$ holds. Here, all the relaxation times T_1, T_2, and $T_{1\rho}$ revealed no dependence on the crystallographic orientation in $\vec{H}_0$. In the second domain, at temperatures below that of the T_1 minimum ($\omega_0\tau \gg 1$), all relaxation times, including T_{1D} exhibited a strong anisotropy.

Sets of results of the detailed angular-dependence studies in the three different samples are presented in Figs. 3–6 in terms of plots of the relaxation times as functions of the polar angle θ. The angle θ was fixed in each case by the crystallographic orientation of the cylindrical axis of the sample. The potassium-doped sample was oriented along its ⟨100⟩ direction, and therefore $\phi = 0°$. The pure and lanthanum-doped samples were oriented with their cylindrical axes along a ⟨110⟩ direction; therefore $\phi = 45°$ for these samples. This latter orientation is particularly favorable for the demonstration of anisotropy since rotation

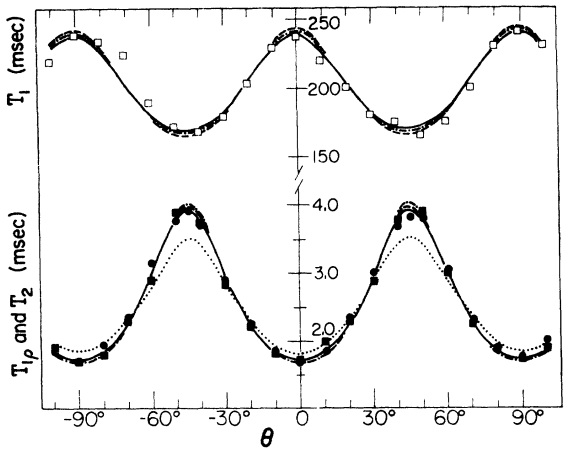

FIG. 3. Orientation dependence of relaxation times in BaF_2:K^+ for $\phi = 0°$ at $1000/T = 1.371$ K^{-1}, where $\omega_0\tau \gg 1$ and $\omega_1\tau \ll 1$ [region (ii)]. □: T_1 at 10 MHz, •: $T_{1\rho}$ at $H_1 = 10$ G, □: T_2 by multiple echo sequence. The solid lines show the computer fits of Eq. (3.1) for T_1 and T_2. The theoretical predictions for the vacancy mechanism (dashed line), and the interstitialcy mechanism (dash-dot line) for T_1 and $T_{1\rho}(=T_2)$, and for the random walk (dotted line) for $T_{1\rho}(=T_2)$ are shown.

about the ⟨110⟩ direction brings all three main crystallographic directions, ⟨100⟩, ⟨110⟩, and ⟨111⟩, parallel to the magnetic field $\vec{H}_0$ in turn, allowing the exploration of the complete range of values of the anisotropy function $f(\theta, \phi)$.

A. Data analysis

As can be seen from the Figs. 3–6, each sample shows pronounced differences in its orientation dependence from one temperature region to another. One method of comparison between regions, which also provides a test of the theoretical predictions, is to evaluate the anisotropy factor Δ defined by Eq. (2.28). The maximum and minimum values of

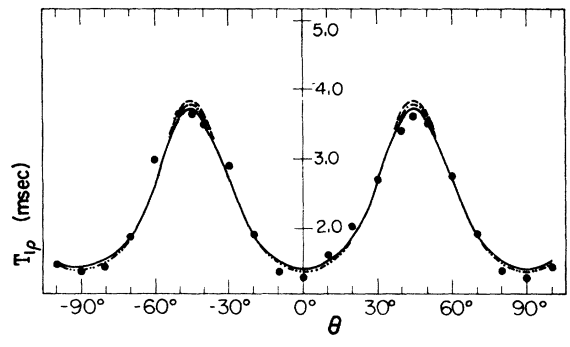

FIG. 4. Orientation dependence of $T_{1\rho}$ ($H_1 = 10$ G) in BaF_2:K^+ for $\phi = 0°$ at $1000/T = 1.925$ K^{-1}, where $\omega_1\tau \gg 1$ [region (iii)]; solid line: computer fit; dashed line: vacancy model; dash-dot line: interstitialcy model.

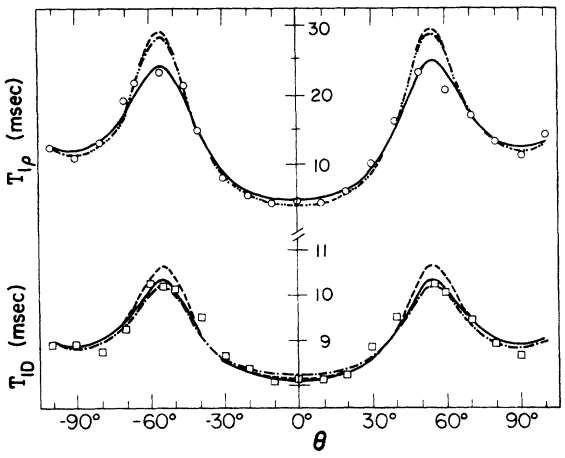

FIG. 5. Orientation dependence of $T_{1\rho}$ ($H_1 = 12$ G) and T_{1D} ($H_1 = 0$) for pure BaF_2, $\phi = 45°$. T_{1D} is shown on an expanded scale. $T_{1\rho}$ at $1000/T = 1.534$ K^{-1} [$\omega_1\tau \gg 1$, region (iii)] and T_{1D} at $1000/T = 1.828$ K^{-1} [$\tau_d \ll T_2^{RL} \ll \tau$, region (iv)]; solid line: computer fit; dashed line: vacancy model; dash-dot line: interstitialcy model.

the relaxation times are most precisely determined by subjecting an entire set of data points to a least-squares-fit analysis. The theoretical expressions for the relaxation times T_1, T_2, and $T_{1\rho}$ in region (i) [Eq. (2.7)], region (ii) [Eqs. (2.12) and (2.9)], and region (iii) [Eqs. (2.12) and (2.16)] may all be written in the general analytic form

$$1/T_r = a_r + f(\theta, \phi) b_r , \tag{3.1}$$

where the parameters a_r and b_r depend on the type of relaxation time, T_r, the diffusion mechanism, and the region considered. A different analytical

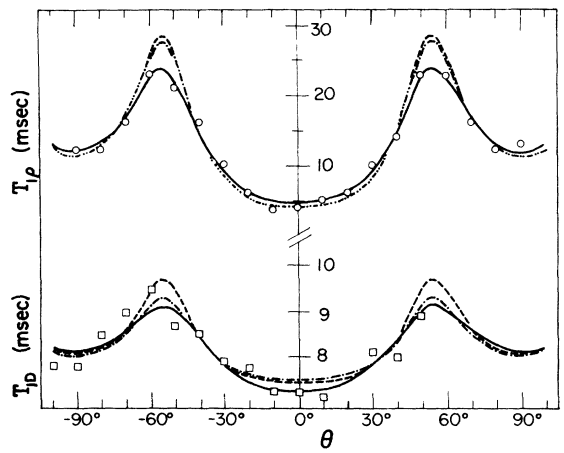

FIG. 6. Orientation dependence of $T_{1\rho}$ ($H_1 = 12$ G) and T_{1D} ($H_1 = 0$) for BaF_2:La^{3+}, $\phi = 45°$. T_{1D} is shown on an expanded scale. $T_{1\rho}$ at $1000/T = 1.880$ K^{-1} [$\omega_1\tau \gg 1$, region (iii)] and T_{1D} at $1000/T = 2.369$ K^{-1} [$\tau_d \ll T_2^{RL} \ll \tau$, region (iv)]; solid line: computer fit; dashed line: vacancy model; dash-dot line: interstitialcy model.

function must be used for region (iv) [Eq. (2.19)], namely

$$\frac{1}{T_{1D}} = \frac{a_D + f(\theta, \phi) b_D}{1 + f(\theta, \phi) c_D} . \tag{3.2}$$

This expression requires a three-parameter fit (but not four). With the aid of a computer program, the parameters in Eqs. (3.1) and (3.2) which minimized the sum of the squared variations for each set of data from corresponding analytical expression were calculated. The parameters so obtained were then used to evaluate the anisotropy factors Δ. This procedure makes no assumption as to the particular type (vacancy, interstitialcy, or even random walk) of diffusion mechanism operating. The values of Δ obtained from the measurements shown in Figs. 3–6 are listed in Table V. The agreement between these values and the theoretical predictions (Table IV) is, in general, very satisfactory.

It will be noted that, particularly when Δ is large, the experimental values tend to be lower than the theoretical values. This is almost certainly due to slight misalignment of the crystal cylinder axis with the assumed axis of rotation. Since (a) the extreme values of the relaxation times would only be obtained if this alignment were in fact true, and (b) measured relaxation times are very sensitive indeed to orientation in this region, slight misalignment will always result in apparently reduced anisotropy factors.

The anisotropies found for the various regions illustrate the main features in the theoretical predictions. The general behavior is as follows:

Region (i) ($\omega_0\tau, \omega_1\tau \ll 1$): Above the T_1 minimum, measurements of T_1, $T_{1\rho}$, and T_2 showed that, at a particular temperature, all were equal and, within experimental accuracy, all were independent of crystal orientation as predicted by Eq. (2.7).

Region (ii) ($\omega_0\tau \gg 1, \omega_1\tau \ll 1$): As predicted by theory, $T_{1\rho}$ and T_2 are equal in this range, and their angular dependence is indistinguishable as shown by the example in Fig. 3. These relaxation times, according to theory, should show a maximum variation with $f(\theta, \phi)$ of $\Delta = 302\%$ or 330% depending on mechanism (Table IV). The experimental values (Table V) are 260% for $T_{1\rho}$ and 300% for T_2 for the curves shown in Fig. 3. These values, although rather low, are much higher than that for a random-walk process, $\Delta = 176\%$ (Table IV). The orientation dependence in T_1 for the same sample at the same temperature is also shown in this region. The magnitude of the variation in T_1 is an order of magnitude less than that found for $T_{1\rho}$ and T_2 in this region. The experimentally determined value of Δ, −36%, from this data is very close to the theoretical values of −38% or −37% (Table IV). This angular dependence for T_1 is seen to be opposite to that of $T_{1\rho}$ and T_2, i.e., T_1 has maxima and minima at the angles for which $T_{1\rho}$ and T_2 have minima and maxima, respectively. This feature is a general result and arises from the nature of the dipole-dipole interaction, different (orthogonal) components of which are selected for the longitudinal (T_1) and transverse ($T_{1\rho}$ and T_2) relaxation processes.

The anisotropies in region (ii) are observed to decrease gradually as the temperature of the T_1 minimum [and region (i)] is approached. This effect can be seen in the $T_{1\rho}$ plots in Fig. 2.

Region (iii) ($\omega_1\tau \gg 1$): In this region, the behavior of T_1 is the same as in region (*ii*), but the orientation dependence of $T_{1\rho}$ is approximately doubled. The $T_{1\rho}$ measurements for all three

TABLE V. Experimentally determined values of the anisotropy factor, Δ (%), and percentage standard deviations for the ^{19}F relaxation times in barium fluoride. For each set of data the standard deviation (i) from the computed best fit to equations (3.1) and (3.2), and (ii) from the theoretical curves for the vacancy and interstitialcy mechanisms are shown.

Sample	Relaxation time	Temperature (K)	Anisotropy factor Δ (%)	Standard deviations (%) Vacancy	Interstitialcy	Computer fit
Pure BaF_2 ($\phi = 45°$)	$T_{1\rho}$ ($\omega_1\tau \gg 1$)	651.9	+420	2.12	1.91	1.81
	T_{1D} ($\tau_d \ll T_2^{RL} \ll \tau$)	547.0	+27	0.226	0.169	0.145
BaF_2 with 0.01-mole% La^{3+} ($\phi = 45°$)	$T_{1\rho}$ ($\omega_1\tau \gg 1$)	531.9	+460	1.94	1.71	0.87
	T_{1D} ($\tau_d \ll T_2^{RL} \ll \tau$)	422.1	+26	0.361	0.323	0.293
BaF_2 with 0.04-mole% K^+ ($\phi = 0°$)	$T_{1\rho}$ ($\omega_1\tau \gg 1$)	519.5	+500	0.153	0.148	0.140
	$T_{1\rho}$ ($\omega_1\tau \ll 1$, $\omega_0\tau \gg 1$)	729.4	+260	0.088	0.108	0.066
	T_2 ($\omega_0\tau \gg 1$)	729.4	+300	0.077	0.083	0.077
	T_1 ($\omega_0\tau \gg 1$)	729.4	−36	0.070	0.068	0.065

samples (Figs. 4–6) show a very large variation with angle θ. The variation is most pronounced for $\phi = 45°$ (Figs. 5 and 6) where the full range of values for $f(\theta, \phi)$ is covered. The relaxation time is found to change by a factor of about 5 ($\Delta \sim 500\%$) which is a little less than the theoretical values shown in Table IV.

Region (iv) ($T_{1\rho}$ for $H_1 \to 0$): The measurements of T_{1D} shown in Figs. 5 and 6 illustrate the typical behavior in the Slichter-Ailion region if the condition $\tau_d \ll T_2^{RL} \ll \tau$ is realized. The values of T_2^{RL} and τ at the temperature of measurement are $T_2^{RL} \simeq 5 \times 10^{-5}$ sec and $\tau \simeq 5 \times 10^{-3}$ sec. Since $\tau_d = (n_d/N)\tau$, where n_d/N is the defect concentration, the value of τ_d may be calculated. For BaF_2 containing 0.01-mole% La^{3+}, $n_d/N = 10^{-4}$ giving $\tau_d \simeq 5 \times 10^{-7}$ sec for this temperature. For pure BaF_2 n_d/N is given by[26,27] $83.9 \exp(-0.96\ \text{eV}/kT)$ and at 547 K has a value of about 10^{-7} giving $\tau_d \simeq 5 \times 10^{-10}$ sec. In both samples, therefore, the condition $\tau_d \ll T_2^{RL} \ll \tau$ under which the encounter model may be applied to the Slichter-Ailion region is clearly satisfied. The orientation dependence of T_{1D} found is very much smaller than that obtained for $T_{1\rho}$ in large fields. The value of Δ thus determined ($\Delta \simeq 26\%$) is close to that predicted by theory (Table IV). As mentioned earlier (Sec. II), angular variation in this region, in contrast to that in regions (i) to (iii), depends only on the terms arising from one single encounter (terms for $S = 1$). Other S terms, in particular, those for $S = 0$ which govern the large local-field anisotropy, do not contribute to the orientation dependence of T_{1D}.

B. Discussion

The results described above show very satisfactory agreement with the general theoretical predictions. The possibilities of using such measurements to identify self-diffusion mechanisms in fluorite crystals will now be considered. Attention will mainly be confined to a comparison between the data and the theoretically predicted angular dependence of relaxation times for the vacancy and interstitialcy mechanisms. The angular dependence as indicated by the theoretical anisotropy factors shown in Table IV, is relatively insensitive to the two mechanisms expected here. The predicted values of Δ for a random-walk model, however, show a significant difference from those for the interstitialcy and vacancy models for T_{1D} [region (iv)] and for T_2 and $T_{1\rho}$ in region (ii) (between the $T_{1\rho}$ and T_1 minima). For this latter region, the experimental results of Table V (Δ = 300% and 260%) clearly favor the two correlated diffusion mechanisms (Δ = 300% and 330%, respectively) rather than a (hypothetical) random-walk mechanism of self-diffusion (Δ = 176%).

An alternative approach is to try to determine which theoretical analytical function (vacancy or interstitialcy) of Table IV fits the data better in each range. The percentage standard deviations of the data points from the fitted curve [Eqs. (3.1) and (3.2)] and the analytical curve for each model (Table IV) were computed. The analytical curves had been normalized to the numerical values of the computer fit at specific values of θ. The results for the three samples studied are presented in Table V. The standard deviations quoted do not include the experimental uncertainty in the relaxation rate or rotation angle. The analytical curves for both correlated mechanisms are shown on Figs. 3–6. The analytical curve for the random-walk model is also plotted on Fig. 3 [region (ii)] and clearly shows a poor agreement with the data.

1. Pure barium fluoride

Measurements of the temperature dependence of ^{19}F relaxation times (Fig. 2) and ionic conductivity[26,27] for these crystals have shown that self-diffusion proceeds by an intrinsic mechanism throughout the temperature range above 500 K, and that aliovalent impurity levels are negligible. From these measurements it is known that both thermally generated F^- vacancies and F^- interstitials (Frenkel defects) are responsible and that the F^- vacancies are more mobile at the lower temperatures where the angular dependence of T_{1D} has been measured. However, while the observed anisotropy factor Δ favors the vacancy model, the standard deviations are lower for the interstitialcy model, although the differences are indeed small. The $T_{1\rho}$ results are equally inconclusive.

2. Doped barium fluoride

Interstitial F^- ions may be introduced into BaF_2 by doping with trivalent cations. La^{3+} was chosen as a dopant since it is not paramagnetic. For temperatures below 750 K, the concentration of F^- interstitials (equal to the concentration of added impurity, viz., 0.01 mole%) is much greater than the concentration of thermally generated Frenkel defects, and temperature-dependence studies indicate an extrinsic interstitialcy-anion self-diffusion mechanism. The results of the orientation-dependence studies of $T_{1\rho}$ at 531.9 K gave values for the anisotropy factor and standard deviation which tend to support this view. However, while the standard deviation for the T_{1D} data at 422.1 K is closer to the optimum fit for the interstitialcy mechanism, the anisotropy factor is in better agreement with that expected for the vacancy mod-

el.

Measurements of $T_{1\rho}$ in the sample doped with monovalent cations (BaF_2:0.04-mole% KF) were made on both sides of the $T_{1\rho}$ minimum ($\omega_1\tau \gg 1$ and $\omega_1\tau \ll 1$) at temperatures for which $T_{1\rho}$ had approximately the same values. The temperature chosen lay well within the extrinsic diffusion region for this sample where F^- diffusion is thought to proceed through the F^- vacancies created by the K^+ impurities.[26,27] The standard deviations of the data from both the vacancy and interstitialcy model for T_1, T_2, and $T_{1\rho}$ are very close to those found for the general computer fit, and are considered to be inconclusive for the precision of these experiments. It is interesting to note that the theoretical anisotropy factors for $T_{1\rho}$ [region (ii)] and T_2 are lower for the vacancy mechanism than for the interstitialcy mechanism, whereas the factors for $T_{1\rho}$ [region (iii)] and T_{1D} are larger for the vacancy case. Since all the measured anisotropy factors for this sample are lower than either of the corresponding theoretical values, it is thought that errors in crystal-axis alignment are obscuring the small differences in Δ that are being sought.

A further complication that arises in the BaF_2:K^+ sample is that ionic-conductivity measurements on it[26,27] show that free F^- vacancy motion dominates over only a very limited range of the high-temperature extrinsic region. The vacancies appear to be trapped by the K^+ impurities as the temperature is reduced. The measured angular dependence would therefore reflect an average over two different types of vacancy movement corresponding to free and impurity-bound vacancies.

The expected differences in crystal-orientation dependence for the two models considered are so small, particularly for T_1, $T_{1\rho}$, and T_2, that the experimental precision required to distinguish between the two correlated diffusion mechanisms is extremely high. The most sensitive relaxation time is T_{1D}, but even here a precision of about 2% is required in its measurement, and the crystal orientation should be accurate to 1° if the differences are to be clearly shown.

IV. CONCLUSIONS

Although the differences in the anisotropy of T_1, T_2, $T_{1\rho}$, and T_{1D} predicted for vacancy and interstitialcy mechansims of diffusion in fluorites were found to require too high an experimental precision for the unambiguous verification of the dominant diffusion mechanism, this theoretical and experimental investigation has confirmed all of the basic predictions of Wolf,[5-8] summarized below:

(i) On the high-temperature side of the T_1 minimum, T_1, T_2, and $T_{1\rho}$ *are* isotropic as first pointed out by Eisenstadt and Redfield.[3]

(ii) On the low-temperature side of the T_1 minimum, T_1 varies in the opposite direction to T_2, $T_{1\rho}$, and T_{1D} as a function of the crystallographic orientation of $\vec{H}_0$.

(iii) On the high-temperature side of the $T_{1\rho}$ minimum, the orientation dependence of $T_{1\rho}$ (for $H_1 \gg H_{D\rho}$) is much less pronounced than on the low-temperature side, where the local-field anisotropy (terms for $S=0$) provides the major contribution to the orientation dependence of $T_{1\rho}$. Owing to the contributions of *many* encounters (terms for $S=0$ to ∞), this rigid-lattice anisotropy is effectively reduced on the high-temperature side, and disappears completely at temperatures above the T_1 minimum.

(iv) In low rotating fields (i.e., the Slichter-Ailion region where $H_1 \leq H_{D\rho}$), the orientation dependence of $T_{1\rho}$ is greatly reduced, and is least for T_{1D} where $H_1 = 0$. If terms for $S=1$ associated with one single encounter were absent, $T_{1\rho}$ would be completely isotropic (see Sec. II A). As H_1 is increased, however, a dramatic increase in the anisotropy factor occurs from about 25 to 500%.

(v) As consequences of the effects (i) to (iv) above, the shapes, widths, and depths of T_1 and $T_{1\rho}$ minima depend on the crystallographic orientation of $\vec{H}_0$. The interpretation of atomic and molecular motion studies by NMR relaxation should take this into account. These effects will be discussed in another article.[9]

The detailed form and magnitude of the orientation dependence of the various relaxation times in the different regions defined in Sec. II A are all well fitted by the appropriate theoretical expressions, the numerical evaluation of which is summarized in Table IV. The general forms of these relations are given by Eqs. (3.1) and (3.2). In particular, the results for T_{1D} with its anisotropy of about 27%, clearly show the anisotropic effects produced by correlated motion on a regular lattice and that the theoretical treatment using the encounter model[6] is most satisfactory. A comparison with the predictions of a simple random-walk model further illustrates that in regions (i) and (iii), i.e., for temperatures above the T_1 minimum and below the high-field $T_{1\rho}$ minimum, respectively, the relaxation behavior is relatively insensitive to mechanism. In region (ii), between the minima, $T_{1\rho}$ and T_2 are much more sensitive to mechanism, and the results for BaF_2 clearly show that a random walk is inappropriate for this material, and that the relative motions of atoms are correlated.

The wide variations with crystal orientation in regions (ii) and (iii) indicate that attempts to determine relaxation times in powders involve an

enormous averaging effect which can introduce large errors,[5-7] and furthermore, experiments on single crystals (with cubic structure) are most reliably performed for $\vec{H}_0$ alignment along ⟨100⟩ crystal axes where inaccuracies in orientation have least effect.

ACKNOWLEDGMENTS

The initial computer calculations were supported by the Institut für Physik at the Max-Planck-Institut für Metallforschung in Stuttgart (West Germany). We are indebted to Dr. C. A. Sholl for making available to us some of his random-walk calculations prior to publication. The experimental work was performed with the assistance of a grant from the Science Research Council (G.B.). Financial support for one of us (D.R.F.) was provided by the Instituto Venezolano de Investigacienes Cientificas, Venezuela.

*Present address: Universidad Simon Bolivar, Departmento De Fisica, Apartado Postal 80659, Caracas, Venezuela.

[1]D. C. Ailion and P. P. Ho, Phys. Rev. 168, 662 (1968).
[2]C. P. Slichter and D. C. Ailion, Phys. Rev. 135, A1099 (1964).
[3]M. Eisenstadt and A. G. Redfield, Phys. Rev. 132, 635 (1963).
[4]H. C. Torrey, Phys. Rev. 92, 962 (1953).
[5]D. Wolf, Phys. Rev. B 10, 2710 (1974).
[6]D. Wolf, Phys. Rev. B 10, 2724 (1974).
[7]D Wolf, J. Magn. Resn. 17, 1 (1975).
[8]D. Wolf, Proceedings of the 18th Ampère Congress, Nottingham 1974 (Nottingham U.P., Nottingham, England, 1975), p. 251.
[9]D. R. Figueroa, J. H. Strange, and D. Wolf (unpublished).
[10]N. Bloembergen, E. M. Purcell, and R. V. Pound, Phys. Rev. 73, 679 (1948).
[11]A. Abragam, *The Principles of Nuclear Magnetism* (Clarendon, Oxford, England, 1962), Chap. VIII.
[12]D. C. Look and I. J. Lowe, J. Chem. Phys. 44, 2995 (1966).
[13]D. Wolf and P. Jung, Phys. Rev. B 12, 3596 (1975).
[14]S. Zumer, Phys. Rev. B 11, 1830 (1975).
[15]D. Wolf and K. Differt, Comput. Phys. Commun. (to be published).
[16]D. Wolf, K. Differt, and H. Mehrer, Comput. Phys. Commun. (to be published).
[17]A. D. LeClaire, in *Physical Chemistry*, edited by H. Eyring, D. Henderson, and W. Jost (Academic, New York, 1970), Vol. X, Chap. 5.
[18]A. B. Lidiard, in *Crystals with the Fluorite Structure*, edited by W. Hayes (Clarendon, Oxford, England, 1974).
[19]P. P. Ho and D. C. Ailion, in Ref. 8, p. 235.
[20]P. P. Ho, thesis (University of Utah, 1973) (unpublished).
[21]D. Wolf, Phys. Rev. B 15, 37 (1977).
[22]C. A. Sholl, J. Phys. C 8, 1737 (1975); W. A. Barton and C. A. Sholl, J. Phys. C 9, 2462 (1976).
[23]H. Y. Carr and E. M. Purcell, Phys. Rev. 94, 630 (1954).
[24]S. Meiboom and D. Gill, Rev. Sci. Instrum. 29, 688 (1958).
[25]J. Jeener, R. Dubois, and P. Broekaert, Phys. Rev. 139, A1959 (1965).
[26]D. R. Figueroa, thesis (University of Kent, United Kingdom, 1976) (unpublished).
[27]D. R. Figueroa, A. V. Chadwick, and J. H. Strange (unpublished).